J Solid State Electrochem (2012) 16:2135–2141
DOI 10.1007/s10008-011-1630-2

ORIGINAL PAPER

# Preparation and electrochemical properties of Zr-doped $LiV_3O_8$ cathode materials for lithium-ion batteries

**Xiangzhong Ren · Shengming Hu · Chuan Shi · Peixin Zhang · Qiuhua Yuan · Jianhong Liu**

Received: 7 September 2011 / Revised: 16 December 2011 / Accepted: 19 December 2011 / Published online: 7 January 2012


**Abstract** The serial Zr-modified lithiated vanadium oxides $LiV_{3-x}Zr_xO_8$ ($x$=0.00, 0.02, 0.04, 0.06, and 0.08) as cathode materials were prepared using a sol–gel method. The synthesized cathode materials have been characterized by X-ray diffraction, scanning electron microscopy, galvanostatic charge–discharge test, cyclic voltammetry, and electrochemical impedance spectroscopy. The results indicate that doped Zr ion does not destroy the lattice structure of $LiV_3O_8$, while enlarging the (100) plane spacing. The discharge–charge tests show that $LiV_{2.94}Zr_{0.06}O_8$ has the best electrochemical properties. The $LiV_{2.94}Zr_{0.06}O_8$ electrode exhibits a high discharge capacity of 269.7 mAh $g^{-1}$ at a charge–discharge rate of 0.1 C in the voltage range of 1.8–4.0 V and maintains a stable capacity of 246.9 mAh $g^{-1}$ within 50 cycles. AC results indicate after $Zr^{4+}$ doping, the charge–transfer resistance and the resistance of lithium-ion diffusion reduce greatly compared to the undoped $LiV_3O_8$, which is favorable to the lithium-ion fast intercalation/deintercalation in bulk materials.

**Keywords** $LiV_3O_8$ · Sol–gel · Cathode materials · Lithium-ion batteries · Zr doping

## Introduction

Lithium trivanadate, as a potential cathode material for rechargeable lithium-ion batteries, has been extensively studied for many years, due to its potentially high reversible capacity, acceptable cyclability, low cost, and facile preparation [1, 2]. It is found that the electrochemical performances of $LiV_3O_8$ cathode material, such as discharge capacity, rate capability, and cycle ability are strongly influenced by the preparation method and posttreatment condition. Numerous synthetic methods have been used including the solid state reaction [3], sol–gel method [4], hydrothermal reactions [5], flame synthesis [6], and ultrasonic treatment techniques [7].

For the successful application of $LiV_3O_8$ as a cathode in lithium-ion batteries, the discharge capacity and cyclability of $LiV_3O_8$ need to be increased. In order to improve the electrochemical performance of $LiV_3O_8$, many cations have been tried to be doped into $LiV_3O_8$. Some cations such as Na, K, Cu, and Ag were doped to substitute lithium [8–11], while other cations such as Mo, Si, Mn, Ni, and Cr were doped to substitute vanadate [12–16]. A small number of anions such as F and Cl were doped to substitute oxygen [17, 18]. After doping, the interlayer distance will undergo an expansion, leading to a much easier lithium-ion intercalation/deintercalation. All of those indicate that doping is an effective method to improve the properties of $LiV_3O_8$.

According to the previous study [19], the capacity fading of lithium trivanadate was ascribed to the local damage of the crystal structure, which was caused by the great change in cell lattice and the partial dissolution of the active material in the liquid electrolyte during the cycling. Zirconium is one of the common dopant materials reported in many literatures [20, 21] because $Zr^{4+}$ is usually believed not to participate in the electrochemical reactions and they can act as a structural pinpoint to maintain the original hexagonal structure during the charge–discharge process.

In this work, Zr was introduced into $LiV_3O_8$ simultaneously as substitutes for V through a sol–gel route (the radius of $Zr^{4+}$ is 61.5 pm, by Zr doping, $Zr^{4+}$ may substitute

X. Ren · S. Hu · C. Shi · P. Zhang (✉) · Q. Yuan · J. Liu
School of Chemistry and Chemical Engineering,
Shenzhen University,
Shenzhen 518060, China
e-mail: pxzhang2000@163.com

$V^{5+}$ (59 pm) which occupies the interlayer site of $LiV_3O_8$ structure). In addition, the effects of Zr substitution on the structural, morphology, and electrochemical properties of $LiV_{3-x}Zr_xO_8$ ($x$=0, 0.02, 0.04, 0.06, and 0.08) compounds were studied in detail.

## Experimental

### Preparation of $LiV_{3-x}Zr_xO_8$ composite

The cathode materials of the layered structure, $LiV_{3-x}Zr_xO_8$ ($x$=0, 0.02, 0.04, 0.06, and 0.08), were prepared by a citrate sol–gel reaction. The starting materials were analytically pure $CH_3COOLi{\cdot}2H_2O$, $NH_4VO_3$, $Zr(NO_3)_4$ and citric acid. Stoichiometric amounts of $CH_3COOLi{\cdot}2H_2O$, $NH_4VO_3$, and $Zr(NO_3)_4$ were accurately weighed. $NH_4VO_3$ (0.03 mol) were dissolved into 100 ml distilled water which was kept in the temperament of 80 °C to form a solution, then, $CH_3COOLi{\cdot}2H_2O$ (0.01 mol) solved into 50 ml distilled water and $Zr(NO_3)_4$ with different molar ratios were added into the solution and stirred for an hour. The citric acid (0.04 mol) solved into 50 ml distilled water was dripped into the mixed solution while stirring slowly. The color of solution changed into nacarat immediately, then varied from nacarat to dark green. Finally, the solution was dried in air at 80 °C to evaporate the water till an orange gel was prepared. The obtained mixed precursors were kept in an oven at 100 °C for 24 h and then calcined at 550 °C for 12 h.

### Characterization of the product

X-ray diffraction (XRD) analysis of the samples was performed using Bruker D8 Advance (Germany) X-ray diffractometer system with graphite monochromatized Cu K$\alpha$ irradiation source in the $2\theta$ range 10–70°, at the scan rate of 1° $min^{-1}$ and voltage of 40 kV. The morphologies of the samples were studied using a scanning electron microscope (SEM), Hitachi model S-3400 N, equipped with Noran instruments (455A-1SPS) for energy dispersive spectroscopy.

### Electrochemical measurements

The composite cathode was prepared by mixing 80 wt.% synthesized $LiV_{3-x}Zr_xO_8$ ($x$=0, 0.02, 0.04, 0.06, and 0.08) with 15 wt.% acetylene black as a conducting agent and 5 wt.% polyvinylidene fluoride as a binder in N-methyl-2-pyrrolidone solvent to form a homogeneous slurry, which was then spread onto an aluminum foil. The coated electrodes were dried in a vacuum oven at 80 °C for 5 h and then pressed into 15 mm wafers. Lithium foils (analytical grade, >99.9%) were used as the anodes. The separator was a microporous membrane (Cellgard 2300 polyethylene (PE)/polypropylene/PE) and the electrolyte used was 1 mol $l^{-1}$ $LiPF_6$ dissolved in a 50/50 vol.% mixture of ethylene carbonate and diethyl carbonate, provided by MERCK. Electrochemical characterizations were carried out using coin cells assembled in an argon-filled glove box (UNILab2000 M. Braun Co.) where the $H_2O$ and $O_2$ concentrations were less than 1 ppm.

Electrochemical cycling tests were performed galvanostatically on a multichannel battery test system (Land BS9300, Wuhan, China) between 1.8 and 4.0 V vs. $Li/Li^+$. A CHI660A electrochemical workstation system (CH Instrument, USA) was used for cyclic voltammetry (scan rate, 0.1 mV $s^{-1}$, 1.8–4.0 V) and electrochemical impedance spectroscopy (EIS) experiments (open circuit potential, amplitude 0.1 mV, $10^5$ to $10^{-2}$ Hz). All the tests were performed at room temperature.

## Results and discussion

The X-ray diffraction patterns of $LiV_{3-x}Zr_xO_8$ ($x$=0, 0.02, 0.04, 0.06, and 0.08) samples are shown in Fig. 1. Table 1 is received by analyzing the XRD data with software of Jade 5.0. It shows that materials can form a solid solution at the range of $0<x<0.08$ as the formula of $LiV_{3-x}Zr_xO_8$. All samples with different amount of $Zr^{4+}$ have very strong diffraction peaks and well-developed structure. Most of which were well matched with the standard JCPDS data (PDF card #72-1193). And all of them have monoclinic structures with the space group $P21/m$. The peak near 12.3° was attributed to $Li_{0.3}V_2O_5$(marked by $^{\nabla}$), which is probably related to the charge compensation [22]. The major difference between the samples with different amount of $Zr^{4+}$ was the relative intensity of the diffraction line corresponding to (100) plane. The peak of (100) plane got weaker with the increase amount of doped $Zr^{4+}$. According to West et al. [23], the low intensity of the (100) line indicates that the crystallization is weak, which would be propitious to gain good electrochemical performance.

The radius of $Zr^{4+}$ is larger than that of $V^{5+}$, so after the intercalation of Zr ion, the interlayer distance increases (see $d_{100}$ values in Table 1,). It shows that the interlayer distance increases monotonously with increasing amount of doping Zr until $x$=0.06. These materials form $LiV_{3-x}Zr_xO_8$ solid solution [24]. When $x$=0.08, the interlayer distance decreased, due to the additive atoms exceeding the solid solution limit.

Elemental mapping of $LiV_{2.94}Zr_{0.06}O_8$ particles was achieved by energy dispersive spectroscopy. Figure 2a shows the SEM of $LiV_{2.94}Zr_{0.06}O_8$ which was chosen to do energy dispersive spectroscopy experiment. Figure 2b–d shows the

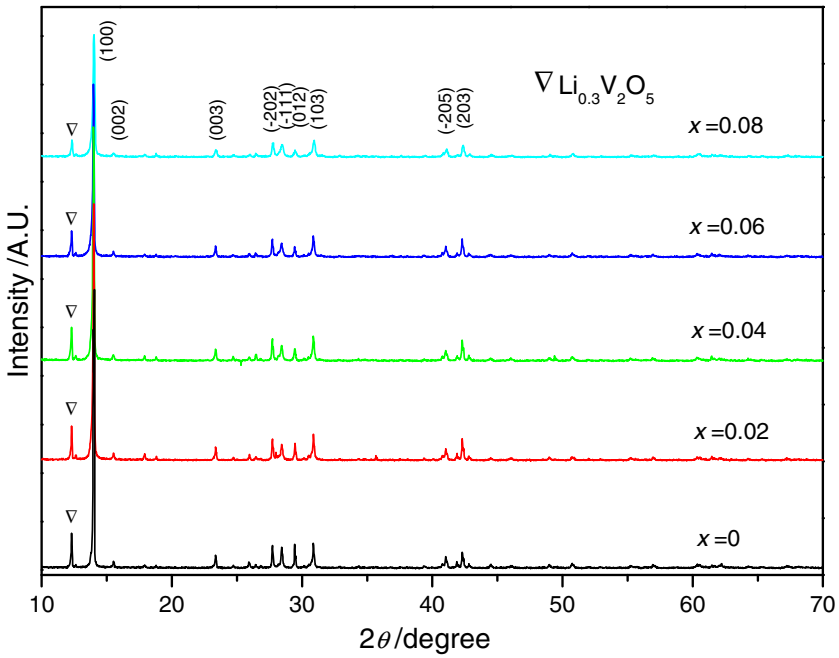


**Fig. 1** XRD pattern of $LiV_{3-x}Zr_xO_8$ ($x$=0, 0.02, 0.04, 0.06, and 0.08)

elemental mapping of V, O, and Zr in $LiV_{2.94}Zr_{0.06}O_8$ compound. A homogeneous distribution of the V, O, and Zr elements was observed in $LiV_{2.94}Zr_{0.06}O_8$ structure with a uniform distribution of the Zr-dopant element on the surface of the individual crystals. This observation confirms the advantages of the sol–gel synthesis process.

Figure 3 shows the initial discharge curves of $LiV_{3-x}Zr_xO_8$ ($x$=0, 0.02, 0.04, 0.06, and 0.08). The shapes of these curves are similar. It can be seen that samples $x$=0 to $x$=0.08 have an initial cycle discharge capacity of 211.7, 235.7, 194.1, 262.7, and 230.3 mAh $g^{-1}$, respectively. Sample $LiV_{0.94}Zr_{0.06}O_8$ has the highest initial discharge capacity. As seen in Fig. 3, there are several charge/discharge plateaus in the voltage profiles whose shapes are similar to each other, which correspond to the intercalation/deintercalation of $Li^+$ ions into/out of the layered materials. There are two main plateaus around 2.8 and 2.5 V, which is the electrochemical characteristic of $Li_{1+x}V_3O_8$ as cathode material [25]. As to sample $LiV_{0.94}Zr_{0.06}O_8$, it can be seen that the main two plateaus almost merge into one plateau. It seems that there is only a smooth slope-like discharge curve, which is a characteristic of amorphous substances [26].

**Table 1** The $d$ and FWHM values of (100) line for $LiV_{3-x}Zr_xO_8$ ($x$=0, 0.02, 0.04, 0.06, and 0.08)

| Sample | $d_{100}$/Å (±0.002) | FWHM/°2Th (±0.002) |
|---|---|---|
| $LiV_3O_8$ | 6.312 | 0.098 |
| $LiV_{2.98}Zr_{0.02}O_8$ | 6.322 | 0.126 |
| $LiV_{2.96}Zr_{0.04}O_8$ | 6.329 | 0.129 |
| $LiV_{2.94}Zr_{0.06}O_8$ | 6.332 | 0.133 |
| $LiV_{2.92}Zr_{0.08}O_8$ | 6.324 | 0.125 |

*FWHM* full width at half maximum

Figure 4 shows the discharge capacity of $LiV_{3-x}Zr_xO_8$ ($x$=0, 0.02, 0.04, 0.06, and 0.08) materials with different contents of doping zirconium at the charge and discharge rates of 0.1 C. It indicates that the zirconium doping would improve the electrochemical performance. It can be seen that the product $LiV_{2.94}Zr_{0.06}O_8$ gives the best cyclability. The $LiV_{2.94}Zr_{0.06}O_8$ electrode shows a high discharge capacity of 269.7 mAh $g^{-1}$ and maintains a capacity of 246.9 mAh $g^{-1}$ after 50 cycles, which is much better than that of the pristine $LiV_3O_8$ (the lower initial discharge capacity and worse cycling stability).

Figure 5 shows the discharge capacity of $LiV_{3-x}Zr_xO_8$ ($x$=0, 0.02, 0.04, 0.06, and 0.08) at a charge–discharge rate of 1.0 C. $LiV_{2.94}Zr_{0.06}O_8$ sample exhibits the highest reversible capacity among the prepared $LiV_{3-x}Zr_xO_8$ ($x$=0, 0.02, 0.04, 0.06, and 0.08) powders. The initial specific discharge capacity of $LiV_{2.94}Zr_{0.06}O_8$ is 169 mAh $g^{-1}$ and still remains 173.1 mAh $g^{-1}$ after 150 cycles. Meanwhile, the initial specific discharge capacity of the undoped material is 139.3 mAh $g^{-1}$ and only remains 124.7 mAh $g^{-1}$ at cycle 150. The $LiV_{2.94}Zr_{0.06}O_8$ sample shows much more improved rate performance than the undoped. Thus, it is obvious that Zr doping significantly improves both a cycling stability and a rate performance especially at higher discharge current densities. These improvements might be caused by higher lithium-ion mobility during charge/discharge processes, which is likely due to the expansion of the crystal's (100) plane spacing. Comparing to the recent work about $LiV_3O_8$, the electrical performance of $LiV_{2.94}Zr_{0.06}O_8$ electrode is excellent [17, 27].

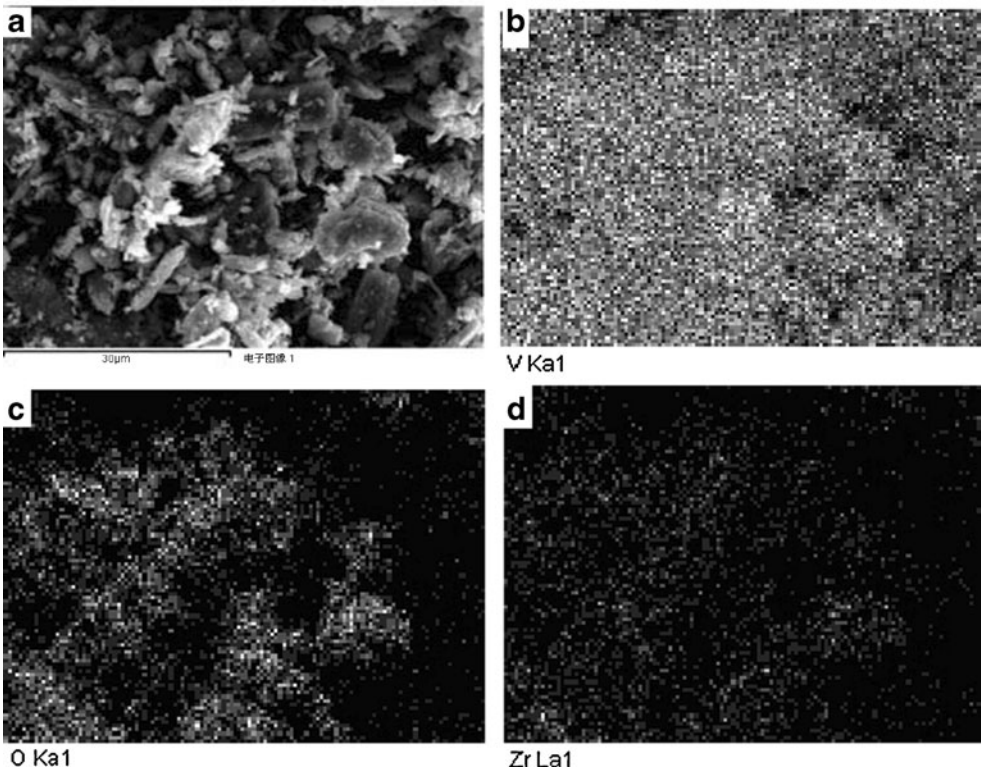


**Fig. 2** SEM micrograph and elemental mapping of $LiV_{2.94}Zr_{0.06}O_8$ (**a**–**d**)

Figure 6 shows the electrochemical performance of $LiV_{3-x}Zr_xO_8$ ($x$=0, 0.02, 0.04, 0.06, and 0.08) at different high temperatures (45 and 60 °C) and a charge–discharge rate of 1.0 C. The results show that the discharge capacity of all samples increase quickly with the temperature arising. The $LiV_{2.94}Zr_{0.06}O_8$ sample shows higher discharge capacity and better cycling ability than the undoped sample.

To provide more information for the improved electrochemical properties, AC impedance measurements are performed on all the samples at the charged state after two cycling. Electrochemical impedance spectroscopies of the fresh electrodes of all the samples were measured in the frequency range from 100 kHz to 10 mHz in a three-electrode cell with lithium foil as counter and reference electrodes. Figure 7 shows the typical Nyquist plots of all samples composite electrodes. All profiles exhibit a semicircle in the high-frequency region and a straight line in the low-frequency region, which are the same as reported in the literature [15]. The high-frequency range corresponds to the double layer response at the electrode/sample interface, and the inclining line in the low-frequency range reflects the diffusion of lithium ions in the solid matrix. The impedance

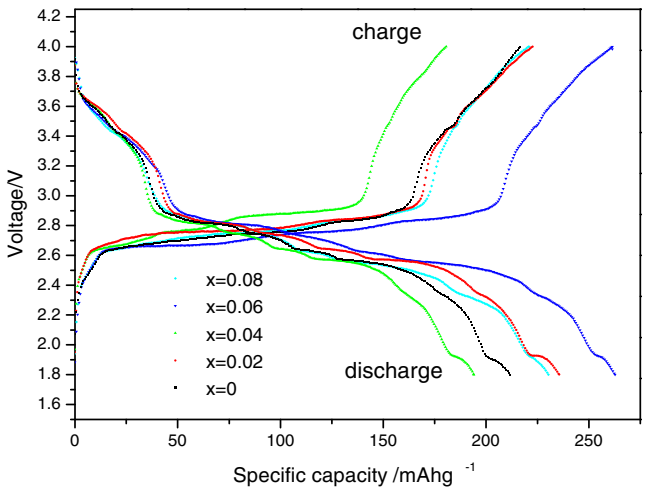


**Fig. 3** Initial charge–discharge curves of $LiV_{3-x}Zr_xO_8$ ($x$=0, 0.02, 0.04, 0.06, and 0.08) (discharge, 4.0–1.8 V at 0.1 C rate)

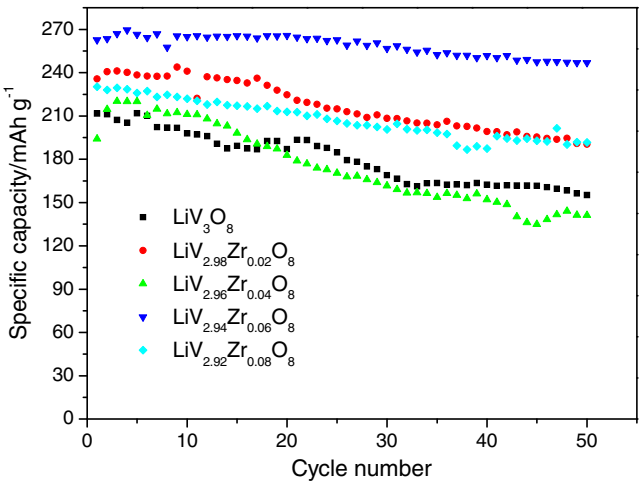


**Fig. 4** Cycle performance of $LiV_{3-x}Zr_xO_8$ ($x$=0, 0.02, 0.04, 0.06, and 0.08) at a charge–discharge rate of 0.1 C

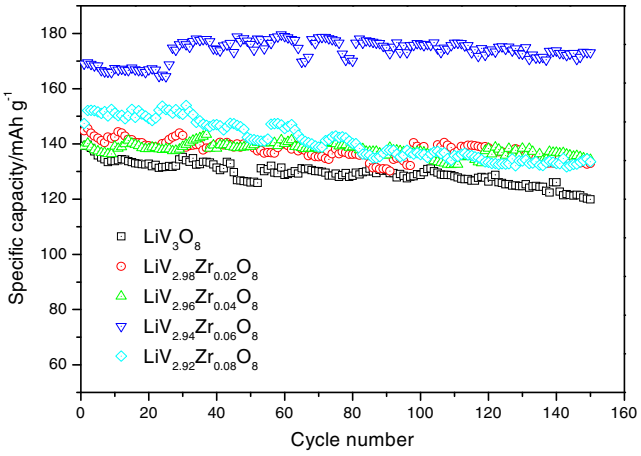


**Fig. 5** Cycle performance of $LiV_{3-x}Zr_xO_8$ ($x$=0, 0.02, 0.04, 0.06, and 0.08) at a charge–discharge rate of 1.0 C

plots were fitted using the equivalent circuit model (Fig. 8), and the fitted impedance parameters were listed in Table 2.

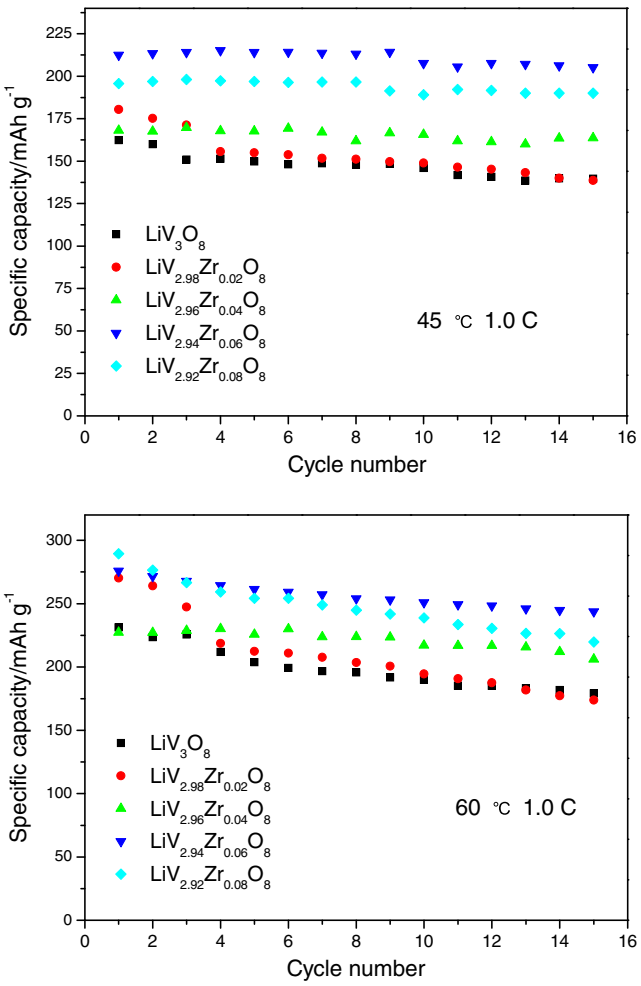


**Fig. 6** Cycling performance of $LiV_{3-x}Zr_xO_8$ ($x$=0, 0.02, 0.04, 0.06, and 0.08) at different high temperatures (45 and 60 °C) and a charge–discharge of 1.0 C

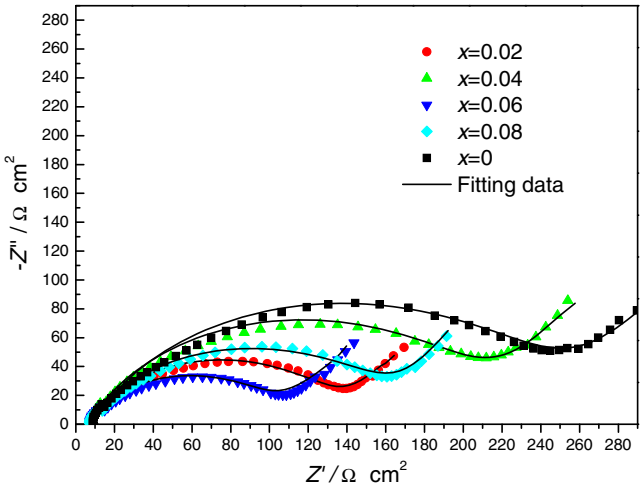


**Fig. 7** Nyquist plots and the fitting data plots at room temperature for $LiV_{3-x}Zr_xO_8$ ($x$=0, 0.02, 0.04, 0.06, and 0.08)

The equivalent circuit model includes electrolyte solution resistance $R_e$, a constant phase element associated with the interfacial resistance, charge–transfer resistance $R_{ct}$, and the Warburg impedance ($Z_w$) related to the diffusion of lithium ions in the solid oxide matrix. The electrolyte solution resistance ($R_e$) values of Zr-doped $LiV_3O_8$ are much lower than those of non-doped $LiV_3O_8$. According to Fey's studies [28] on EIS of lithium-ion cells, solution resistance ($R_e$) is not an important factor for the charge–discharge process because it is independent of the voltage at which the measurements were made. The charge–transfer resistance ($R_{ct}$) values of Zr-doped $LiV_3O_8$ are much lower than those of non-doped $LiV_3O_8$, and the same result can be seen in the EIS fitting data. From Fig. 7, it is obvious that there is a remarkable decrease in $R_{ct}$ after Zr doping, indicative of the increase of the conductivity of Zr-doped $LiV_3O_8$ as compared to that of $LiV_3O_8$. The charge–transfer resistance ($R_{ct}$) value of $LiV_{2.94}Zr_{0.06}O_8$ is lowest of all, which is in agreement with its best electrochemical characteristics. What is more, the Warburg impedance decreases greatly after Zr doping. It means the lithium ion is easier to diffuse in the solid oxide matrix.

AC impedance measurements at different temperatures (45 and 60 °C) are performed on all the samples at the charged state after two cycling. Electrochemical impedance spectroscopies of the fresh electrodes of all the samples were measured in the frequency range from 100 kHz to 10 mHz in a three-electrode cell with lithium foil as counter

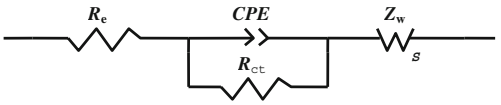


**Fig. 8** Equivalent circuit used to model EIS data of $LiV_{3-x}Zr_xO_8$ ($x$=0, 0.02, 0.04, 0.06, and 0.08)

**Table 2** Impedance parameters for $LiV_{3-x}Zr_xO_8$ ($x$=0, 0.02, 0.04, 0.06, and 0.08)

| Sample | $R_e$/Ω cm$^2$ (±0.4) | $R_{ct}$/Ω cm$^2$ (±6) | $Z_w$/Ω cm$^2$ (±8) |
|---|---|---|---|
| $LiV_3O_8$ | 8.3 | 238 | 1,356 |
| $LiV_{2.98}Zr_{0.02}O_8$ | 6.6 | 127 | 383 |
| $LiV_{2.96}Zr_{0.04}O_8$ | 5.6 | 203 | 434 |
| $LiV_{2.94}Zr_{0.06}O_8$ | 6.0 | 94 | 404 |
| $LiV_{2.92}Zr_{0.08}O_8$ | 6.0 | 157 | 389 |

and reference electrodes. Figure 9 shows the typical Nyquist plots of all samples composite electrodes at different temperatures (45 and 60 °C). The charge–transfer resistance ($R_{ct}$) values of samples $x$=0 to $x$=0.08 are about 101, 64, 69, 48, and 60 Ω cm$^2$, respectively, at 45 °C. Their values reduce to about 80, 27, 35, 19, and 21 Ω cm$^2$, respectively, at 60 °C. The charge–transfer resistance ($R_{ct}$) values of all sample reduce greatly with the temperature arising. High temperature is favorable to the lithium-ion fast intercalation/deintercalation in bulk materials. Combine with the electrochemical performance data of $LiV_{3-x}Zr_xO_8$ ($x$=0, 0.02, 0.04, 0.06, and 0.08) at different high temperatures, the charge–transfer resistance ($R_{ct}$) value varies inversely with the third discharge capacity to some extent.

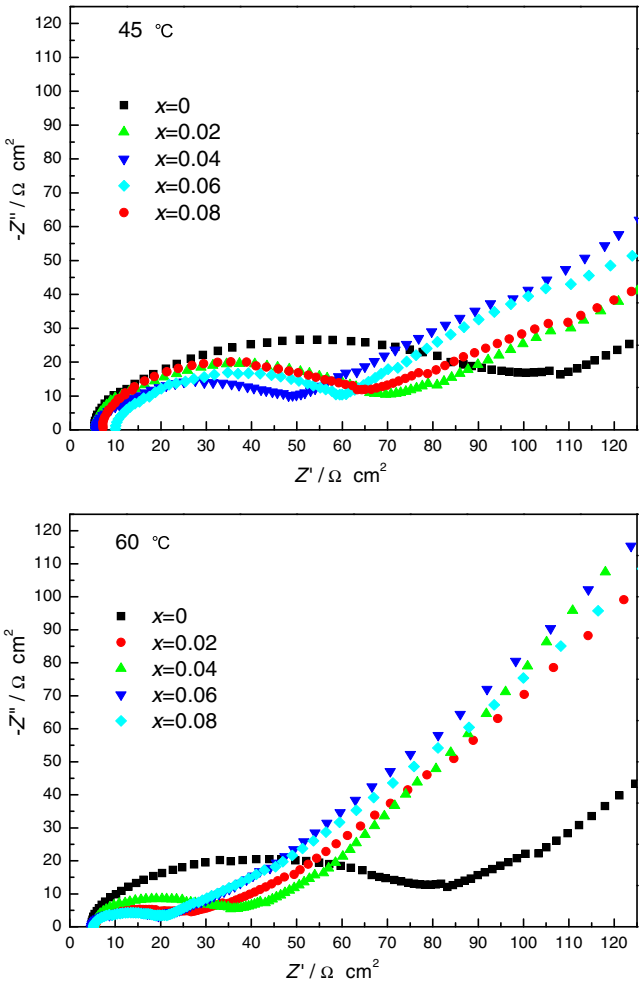


**Fig. 9** Nyquist plots at different high temperatures (45 and 60 °C) for $LiV_{3-x}Zr_xO_8$ ($x$=0, 0.02, 0.04, 0.06, and 0.08)

Figure 10 shows the third cyclic voltammograms of $LiV_{3-x}Zr_xO_8$ ($x$=0, 0.02, 0.04, 0.06, and 0.08) measured at a scan rate of 0.1 mV s$^{-1}$ in the voltage range of 1.8–4.0 V at room temperature. For $LiV_3O_8$, there are four main anodic peaks at 2.52, 2.82, 2.86, and 3.69 V (vs. Li/Li$^+$) and several main cathodic peaks at 3.63, 2.79, 2.70, 2.63, and 2.52 V (vs. Li/Li$^+$) present, which indicates multiple discharge plateaus. The doped materials also have similar anodic and cathodic peaks, but the peak position and its intensity are slight different. The anodic peaks of sample $x$=0.04 are larger and lower than those of undoped sample. What is more, the anodic peaks of sample $x$=0.02 and $x$=0.08 are larger and higher than those of undoped sample. After doping, the anodic peaks around 2.82 V of doped sample shifted toward lower potential than those of undoped sample. For the doped material $LiV_{2.94}Zr_{0.06}O_8$, the peak areas are the largest and the difference between the potentials of predominant anodic and cathodic peak are the smallest of all the materials tested. It concludes that $LiV_{2.94}Zr_{0.06}O_8$ has the highest specific charge–discharge capacity and holds the best reversibility, in agreement with that obtained from the charge–discharge cycle test at 0.1 C.

## Conclusion

In this work, a series of Zr-modified lithiated vanadium oxides ($LiV_{3-x}Zr_xO_8$, $x$=0.00, 0.02, 0.04, 0.06, and 0.08) were prepared by a sol–gel method, and the impacts of the zirconium substitution for V in $LiV_3O_8$ on the electrochemical properties

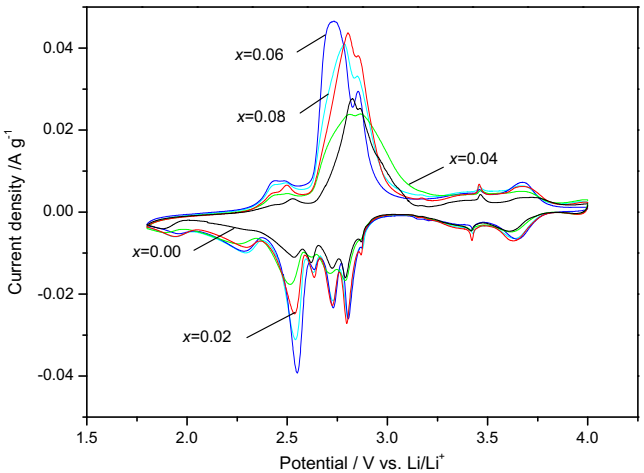


**Fig. 10** The third cyclic voltammograms of $LiV_{3-x}Zr_xO_8$ ($x$=0, 0.02, 0.04, 0.06, and 0.08)

and conductivity have been investigated. The results reveal that the zirconium doping tends to increase the interlayer spacing of the bulk material and make it more stable during charge–discharge cycling, which may improve the electrochemical performance significantly. Compared with undoped $LiV_3O_8$, $LiV_{2.94}Zr_{0.06}O_8$ shows higher discharge capacity, better cycling stability (the discharge capacity remains 252.7 mAh $g^{-1}$ even after 50 cycles), and lower impedance. The charge–transfer resistance ($R_{ct}$) value varies inversely with the third discharge capacity to some extent. Overall, zirconium substitution is an effective way to improve the electrochemical performance of $LiV_3O_8$ cathode materials.

**Acknowledgments** Financial supports for this work were provided by the National Natural Science Foundation of China (grant #50974090, 50874074) and the Shenzhen Key Laboratory of New Lithium-ion Battery and Mesoporous Materials (20110201).

## References

1. West K, Zachau C (1996) J Electrochem Soc 143:820–825
2. Dai J, Li F, Gao Z, Siow K (1998) J Electrochem Soc 145:3057–3062
3. Kannan A, Manthiram A (2006) J Power Sources 159:1405–1408
4. Liu L, Jiao L, Zhang Y, Sun J, Yang L, Miao Y, Yuan H, Wang Y (2008) Mater Chem Phys 111:565–569
5. Liu H, Wang Y, Wang K, Wang Y, Zhou H (2009) J Power Sources 192:668–673
6. Ju S, Kang Y (2010) Electrochim Acta 55:6088–6092
7. Yang G, Wang G, Hou W (2005) J Phys Chem B 109:11186–11196
8. Pasquali M, Pistoia G (1991) Electrochim Acta 36:1549–1553
9. Pistoia G, Wang G, Zane D (1995) Solid State Ionics 76:285–290
10. Jiao L, Li H, Yuan H, Wang Y (2008) Mater Lett 62:3937–3939
11. Feng C, Huang L, Guo Z, Wang J, Liu H (2007) J Power Sources 174:548–551
12. Pouchko S, Ivanov S, Kulova T, Skundin A, Turevskaya E (2002) Solid State Ionics 151:129–140
13. Zhao M, Jiao L, Yuan H, Feng Y, Zhang M (2007) Solid State Ionics 178:387–391
14. Liu L, Jiao L, Sun J, Zhao M, Zhang Y, Yuan H, Wang Y (2008) Solid State Ionics 178:1756–1761
15. Liu L, Jiao L, Sun J, Zhang Y, Zhao M, Yuan H, Wang Y (2008) Electrochim Acta 53:7321–7325
16. Feng Y, Li Y, Hou F (2009) Mater Lett 63:1338–1340
17. Liu Y, Zhou X, Guo Y (2009) Electrochim Acta 54:3184–3190
18. Liu L, Jiao L, Sun L, Liu S, Yuan H, Wang Y (2009) Chin J Chem 27:1093–1098
19. Jouanneau S, Gal La Salle A, Verbaere A, Guyomard D (2005) J Electrochem Soc 152:1660–1667
20. Oh S, Lee S, Cho W, Cho B (2006) Electrochim Acta 51:3637–3644
21. Kim S, Kim C (2009) J Electroceram 23:254–257
22. Kawakita J, Katagiri H, Miura T, Kishi T (1997) J Power Sources 68:680–685
23. West K, Zachau C, Skaarup S, Saidi M, Barker Y, OIsen I, Pynenburg R, Koksbang R (1996) J Electrochem Soc 141:820–825
24. Zhang H, Tang Y, Shen J, Xin X, Cui L, Chen L, Ouyang C, Shi S, Chen L (2011) Appl Phys A 104:529–537
25. Wu F, Wang L, Wu C, Bai Y, Wang F (2009) Mater Chem Phys 115:707–711
26. Feng C, Wang S, Zeng R, Guo Z, Konstantinov K, Liu H (2008) J Power Sources 184:485–488
27. Sakunthala A, Reddy MV, Selvasekarapandian S, Chowdari BVR, Christopher Selvin P (2010) J Phys Chem C 114:8099–8107
28. Fey G, Chen J, Subramanian V, Osaka T (2002) J Power Sources 112:384–394